Finite Temperature Phase Behavior of Viral Capsids as Oriented Particle Shells: Supplementary Material

Amit Singh[1], Andrej Košmrlj[2,3], and Robijn Bruinsma[4]
[1]*Department of Physics and Astronomy, Johns Hopkins University, Baltimore, MD 21218, USA*
[2]*Department of Mechanical and Aerospace Engineering, Princeton University, Princeton, NJ 08540, USA*
[3]*Princeton Institute for the Science and Technology of Materials (PRISM), Princeton University, Princeton, NJ 08544, USA and*
[4]*Departments of Physics and Astronomy, and Chemistry and Biochemistry, University of California, Los Angeles, CA 90095, USA*

I. NUMERICAL METHODS.

A. Variational Method

The finite temperature simulations of the OPS were based on an iterative solution of the coupled discretized Langevin equations

$$\frac{\partial U^{n+1}}{\partial \mathbf{r}_i^{n+1}} + \frac{k_B T}{D}\frac{(\mathbf{r}_i^{n+1} - \mathbf{r}_i^n)}{\Delta t} - k_B T\sqrt{\frac{2}{D\Delta t}}\boldsymbol{\xi}_i^{n+1} = 0, \tag{S1}$$

for the particle locations. At every time step, all particle locations and orientations were updated in parallel. Here, n is the time index with discrete time step Δt, $U^{n+1} = \frac{1}{2}\sum_{i\neq j} V(\mathbf{r}_i^{n+1}, \mathbf{n}_i^{n+1}; \mathbf{r}_j^{n+1}, \mathbf{n}_j^{n+1})$ the total potential energy associated with OPS pair interaction Eq. (S1) at time step $n+1$. D is the translational diffusion coefficient and the $\boldsymbol{\xi}_i^n$ are a set of $3N$ Gaussian random variables with variance one. The orientational degrees at time step $n+1$ were obtained by demanding that the torques

$$\boldsymbol{\tau}_i^{n+1} \equiv \mathbf{n}_i^{n+1} \times \frac{\partial U^{n+1}}{\partial \mathbf{n}_i^{n+1}} = 0 \tag{S2}$$

on the particle orientations vanished at every time step. Physically, "integrating-out" of the orientational degrees of freedom produces an effective interaction between the remaining translational degrees of freedom of the N point particles. The effective interaction is no longer the sum of radial pair interactions between neighboring point particles but now incudes more complex 3-body and higher-order interactions and longer-range interactions mediated by the orientational degrees of freedom.

At every time step, the set of $5N$ equations for the same number of unknowns $\mathbf{r}_i^{n+1}$ and $\mathbf{n}_i^{n+1}$ was solved by numerical minimization of the expression

$$\begin{aligned} I^{n+1} &= U^{n+1} + \left(\frac{k_B T}{2D\Delta t}\right)\sum_i \left(\mathbf{r}_i^{n+1} - \mathbf{r}_i^n\right)^2 \\ &- k_B T\sqrt{\frac{2}{D\Delta t}}\sum_i \boldsymbol{\xi}_i^{n+1}\cdot\left(\mathbf{r}_i^{n+1} - \mathbf{r}_i^n\right). \end{aligned} \tag{S3}$$

where, as before, the superscripts $n+1$ and n denote time-steps. The minimization of I^{n+1} with respect to $\mathbf{n}_i^{n+1}$ was of course restricted to rotations, which leads to Eq. (S2). The successive rotations were stored in the form of rotation vectors perpendicular to the orientation vectors. The orientations were reconstructed from the rotation vectors using the method of quaternions [1].

B. Area Constraint

In order to suppress evaporation of single particles from the cell we imposed a soft fixed area constraint using the Augmented-Lagrangian (AL) technique as follows. The constrained minimization problem is finding

the minimum of I^{n+1} subject to the constraint $A\left(\mathbf{r}^{n+1}\right) - A_0 = 0$ where A_0 is the zero-temperature area and $A\left(\mathbf{r}^{(n+1)}\right) \equiv A^{n+1}$ is the area after $n+1$ time steps. Introduce a Lagrange multiplier term and an augmenting penalty term as follows

$$F[\mathbf{r}^{(n+1)}, \mathbf{n}^{(n+1)}] = I^{n+1} + \frac{k^{n+1}}{2}\left(A^{n+1} - A_0\right)^2 - \lambda^{n+1}\left(A^{n+1} - A_0\right) \tag{S4}$$

where k^{n+1} is an estimate of the spring constant of the penalty term at time step $n+1$ and λ^{n+1} is an estimate of the Lagrange multiplier at time step $n+1$. For a given time step, successive estimates are updated according to

1. Set $k^{(n+1)} = 1000.0$ and $\lambda^{(n+1)} = 10.0$.
2. Find $\mathbf{r}^{(n+1)}, \mathbf{n}^{(n+1)} = \text{argmin } F[\mathbf{r}^{(n+1)}, \mathbf{n}^{(n+1)}]$
3. While $\left(A^{(n+1)} - A_0\right) > 10^{-8}$, repeat
   (a) $\lambda^{(n+1)} \leftarrow \lambda^{(n+1)} - k^{(n+1)}\left(A^{(n+1)} - A_0\right)$
   (b) $k^{(n+1)} \leftarrow 10 \times k^{(n+1)}$
   (c) Find $\mathbf{r}^{(n+1)}, \mathbf{n}^{(n+1)} = \text{argmin } F[\mathbf{r}^{(n+1)}, \mathbf{n}^{(n+1)}]$

At the end of this procedure the area constraint is satisfied to a desired tolerance. The advantage of Augmented Lagrangian method over the standard method of Lagrange multipliers is that one does not need to introduce an extra degree of freedom. The Augmented Lagrangian parameters k and λ are solved iteratively in a loop external to the regular time step updating. The parameter $k^{(n+1)}$ does not need to go to infinity and thus numerical ill-conditioning is avoided.

C. Simulation Details

Equation (S3) can be written in non-dimensionalized form as

$$\begin{aligned} I[\mathbf{r}^{(n+1)}, \mathbf{n}^{(n+1)}] &= \sum_{i \neq j}\left(e^{-2\alpha(|\mathbf{r}_{ij}|-a)} - 2e^{-\alpha(|\mathbf{r}_{ij}|-a)}\right) \\ &+ \frac{2\alpha^2 R^2}{3\gamma}\left(\sum_{i\neq j}|\mathbf{n}_i - \mathbf{n}_j|^2 + \sum_{i\neq j}\left(\frac{(\mathbf{n}_i + \mathbf{n}_j)\cdot\mathbf{r}_{ij}}{|\mathbf{r}_{ij}|}\right)^2\right) \\ &+ \frac{\zeta}{a^2}\frac{\left(\mathbf{r}^{(n+1)} - \mathbf{r}^{(n)}\right)^2}{2} - \frac{1}{a}\sqrt{\frac{2\zeta}{\beta}}\,\hat{\boldsymbol{\xi}}_r \cdot \left(\mathbf{r}^{(n+1)} - \mathbf{r}^{(n)}\right) \end{aligned} \tag{S5}$$

V_M, α and a are parameters of the Morse potential that control the depth, the width and the equilibrium separation respectively. R is the radius of the shell. K controls the strength of the orientational potentials. μ is the mobility. The three non-dimensional parameters are given as

$$\begin{aligned} \beta &= \frac{V_M}{k_B T}, \\ \gamma &= \frac{2\alpha^2 R^2 V_M}{3K}, \\ \zeta &= \frac{a^2}{V_M}\frac{1}{\mu\Delta t}. \end{aligned} \tag{S6}$$

The interactions between the particles are restricted to the nearest neighbors that were obtained via a triangulation of the shell surface by first projecting all particles to a sphere and then constructing the

convex hull of the particle array. The set of nearest neighbors consists of particles that share an edge in the triangulation.

The width of the Morse potential can be expressed as $\delta = \ln 2/(\alpha a)$ and we previously demonstrated that it must be larger than a critical value for the formation of stable shells at low FvK numbers. [2] In practice, we found that $\delta = 0.15$ was sufficiently large and thus we chose $\alpha a = \ln 2/0.15 = 4.621$.

We chose 30 log-spaced values of FvK number (γ) between 0.2 and 20000. For each FvK number, we used 20 temperature ($1/\beta$) values. ζ is kept fixed at 2.5×10^5. For each combination of FvK number and temperature we did 3 runs where each run comprised of evolving the system for 2×10^6 time steps starting from the zero-temperature minimum energy structure for the specific FvK number. After every time-step we "subtract" off the rigid body translation and rotation with respect to the initial structure using the Kabsch algorithm [3].

D. Simulation Output

At every time step, we stored the means of the squared relative neighbor-neighbor displacement for all particles, which is calculated as follows. Suppose that particles i and j were the nearest neighbors at time $t = 0$, then the squared relative displacement is given by $\|(\mathbf{r}_i(t) - \mathbf{r}_i(0)) - (\mathbf{r}_j(t) - \mathbf{r}_j(0))\|^2$. We cannot use displacement of individual particles $\|\mathbf{r}_i(t) - \mathbf{r}_i(0)\|^2$ because for 2D melting it diverges and relative neighbor-neighbor displacement provides the appropriate modification to the Lindemann criterion [4].

We also stored, the asphericity, the volume and the root mean-squared angle deficit of the shell. The asphericity is defined as $\langle (R_i - \langle R_i \rangle)^2 \rangle / \langle R_i \rangle^2$ where R_i is the radial distance of particle i from center of the shell. For calculating volume and root-mean-squared angle deficit, we need a triangulation of the surface of the shell defined by the particles. We calculate the triangulation by projecting each particle to a unit sphere and calculating the convex hull of the spherical point cloud using CGAL [5] software package. The angle deficit is a measure of Gaussian curvature of the surface and it is calculated as discussed in [6].

We also store the particle positions and orientations after every 2000 time steps. We use this to reconstruct the shell shape during post-processing to detect crumpling of the shells.

E. Software

The minimizations were carried out using the Limited Memory BFGS [7] algorithm and the code used is available publicly on `https://github.com/amit112amit/ops-python`, in the form of a Python wrapped C++ code. The main driver used for the simulations is `phasediagramsimulation.py` located at `https://github.com/amit112amit/ops-python/blob/master/phasediagramsimulation.py`. The results of these simulations are publicly available as an interactive Jupyter notebook at `https://mybinder.org/v2/gh/amit112amit/opsresults/master?filepath=ShowPlots.ipynb`.

II. THIN-SHELL ELASTICITY THEORY

In this section we discuss how to calculate the spectrum of in-plane and out-of-plane fluctuations within the harmonic regime of the thin-shell elasticity theory. First, we discus the continuum limit, where the radius R of the spherical shell is assumed to be much larger than its thickness t. Second, we discuss how to take into account finite size effects.

A. Large shell limit

As shown previously in refs. [8, 9], the relevant length scale for the statistical mechanics of thin shells is the elastic length scale $\ell_{\text{el}} = R\gamma^{-1/4} \sim \sqrt{Rt}$, where $\gamma = YR^2/\kappa$ is the FvK number. (Y is the Young's modulus, κ is the bending rigidity). For thin shells $\gamma \gg 1$ and thus $\ell_{\text{el}} \ll R$. In this limit it is sufficient to consider a small square patch of spherical shell, which is much larger than ℓ_{el} and much smaller than R [8, 9].

Deformation of a small spherical patch is described with displacement vector fields, which are decomposed into the outward radial displacement field $f(\mathbf{x})$ and the tangential displacements $u_i(\mathbf{x})$, where $\mathbf{x} = (x_1, x_2)$

and $i \in \{1,2\}$. The total deformation energy of a small patch consists of the bending energy cost

$$U_{\rm b} = \int dA\ \frac{1}{2}\kappa \left(\Delta f\right)^2, \tag{S7}$$

where κ is the bending rigidity, and the stretching energy cost

$$U_{\rm s} = \int dA \left[\frac{1}{2}\lambda u_{ii}^2 + \mu u_{ij}^2\right], \tag{S8}$$

where λ and μ are Lame elastic constants with the Young's modulus $Y = 4\mu(\mu+\lambda)/(2\mu+\lambda)$ and the summation over repeated indices is implied. Here, we introduced the strain tensor

$$u_{ij} = \frac{1}{2}\left(\partial_i u_j + \partial_j u_i\right) + \delta_{ij}\ \frac{f}{R}, \tag{S9}$$

where δ_{ij} is the Kronecker delta. Since we are only focusing on the harmonic spectrum of fluctuations, we neglected the nonlinear term $(\partial_i f)(\partial_j f)/2$ in the strain tensor u_{ij}, which becomes relevant, when the amplitude of fluctuations becomes larger than the shell thickness [9].

The spectrum of fluctuations can be analyzed with the help of Fourier transforms $f(\mathbf{x}) = \sum_{\mathbf{q}} f(\mathbf{q}) e^{i\mathbf{q}\cdot\mathbf{x}}$ and $u_i(\mathbf{x}) = \sum_{\mathbf{q}} u_i(\mathbf{q}) e^{i\mathbf{q}\cdot\mathbf{x}}$. Furthermore, we use the Helmholtz decomposition for the in-plane displacements $\mathbf{u}(\mathbf{q}) = \mathbf{u}_\parallel(\mathbf{q}) + \mathbf{u}_\perp(\mathbf{q})$, where $\mathbf{u}_\parallel \parallel \mathbf{q}$ and $\mathbf{u}_\perp \perp \mathbf{q}$. Using this decomposition we rewrite the total deformation energy as

$$\begin{aligned} U_{\rm b} + U_{\rm s} = A\sum_{\mathbf{q}} \Bigg(&\frac{1}{2}\kappa q^4 |f(\mathbf{q})|^2 + \frac{1}{2}(2\mu+\lambda) q^2 |\mathbf{u}_\parallel(\mathbf{q})|^2 + \frac{1}{2}\mu q^2 |\mathbf{u}_\perp(\mathbf{q})|^2 + 2\frac{(\mu+\lambda)}{R^2}|f(\mathbf{q})|^2 \\ &+ i\frac{(\mu+\lambda)}{R}\left[\mathbf{q}\cdot\mathbf{u}_\parallel(\mathbf{q})\right] f(-\mathbf{q}) - i\frac{(\mu+\lambda)}{R}\left[\mathbf{q}\cdot\mathbf{u}_\parallel(-\mathbf{q})\right] f(\mathbf{q})\Bigg). \end{aligned} \tag{S10}$$

The spectrum of thermal fluctuations is thus

$$\left\langle |f(\mathbf{q})|^2 \right\rangle = \frac{k_B T}{A(\kappa q^4 + Y/R^2)}, \tag{S11a}$$

$$\left\langle |\mathbf{u}_\perp(\mathbf{q})|^2 \right\rangle = \frac{k_B T}{A\mu q^2}, \tag{S11b}$$

$$\left\langle |\mathbf{u}_\parallel(\mathbf{q})|^2 \right\rangle = \frac{k_B T(4(\mu+\lambda) + \kappa q^4 R^2)}{A(Yq^2 + \kappa q^6 R^2)(2\mu+\lambda)}, \tag{S11c}$$

where T is temperature, k_B the Boltzmann constant, and A the area of the small spherical patch. The total amplitude of out-of-plane fluctuations can then be obtained as

$$\left\langle f(\mathbf{x})^2 \right\rangle = \sum_{\mathbf{q}} \left\langle |f(\mathbf{q})|^2 \right\rangle \approx A\int \frac{d^2\mathbf{q}}{(2\pi)^2} \left\langle |f(\mathbf{q})|^2 \right\rangle \approx A\int_{\pi/R}^{\pi/a} \frac{q dq}{(2\pi)} \left\langle |f(q)|^2 \right\rangle \equiv \frac{k_B T}{Y} G_\infty^f(\gamma), \tag{S12a}$$

$$G_\infty^f(\gamma) \approx \begin{cases} \sqrt{\gamma}/(2\pi), & a \ll \ell_{el} \ll R \\ (\pi/4)(R/a)^2, & \ell_{el} \ll a \ll R \end{cases}, \tag{S12b}$$

where a is the microscopic cutoff related to the interparticle spacing. Similarly, we calculate the total amplitude of in-plane fluctuations as

$$\left\langle \mathbf{u}(\mathbf{x})^2 \right\rangle = \sum_{\mathbf{q}} \left(\left\langle |\mathbf{u}_\parallel(\mathbf{q})|^2 \right\rangle + \left\langle |\mathbf{u}_\perp(\mathbf{q})|^2 \right\rangle\right) \approx A\int_{\pi/R}^{\pi/a} \frac{q dq}{(2\pi)} \left(\left\langle |\mathbf{u}_\parallel(q)|^2 \right\rangle + \left\langle |\mathbf{u}_\perp(q)|^2 \right\rangle\right) \equiv \frac{k_B T}{Y} G_\infty^u(\gamma), \tag{S13a}$$

$$G_\infty^u(\gamma) \approx \begin{cases} (2/9\pi)\left[\ln(\gamma) + 8\ln(R/a)\right], & a \ll \ell_{el} \ll R \\ (8/3\pi)\ln(R/a) & \ell_{el} \ll a \ll R \end{cases}, \tag{S13b}$$

where we used $\mu = \lambda = 3Y/8$ that corresponds to the continuum limit of the OPS.

B. Finite size effects

In order to capture the finite size effects for small shells composed of N particles, we have to consider deformations of the whole spherical shell, which are decomposed into the outward radial displacement field $f(\theta,\phi)$ and the tangential displacements $u_\alpha(\theta,\phi)$, where $\alpha \in \{\theta,\phi\}$. The Helmholtz decomposition is used for tangential displacements to separate the irrotational and the solenoidal part as [10]

$$u_\alpha = D_\alpha \psi + \gamma_{\alpha\beta} D^\beta \chi. \tag{S14}$$

Here D_α are covariant derivatives and $\gamma_{\alpha\beta}$ is the alternating tensor, which depends on the metric and can be expressed as $\gamma_{\alpha\beta} = \sqrt{g}\epsilon_{\alpha\beta}$, where g is the determinant of the metric tensor $g_{\alpha\beta}$ and $\epsilon_{\alpha\beta}$ is the antisymmetric Levi-Civita symbol. Indices are raised and lowered with the metric tensor $g_{\alpha\beta}$. The tangential displacements can thus be described with two fields $\psi(\theta,\phi)$ and $\chi(\theta,\phi)$. The 3 scalar fields describing displacements can be expanded in spherical harmonics as

$$\begin{aligned} f(\theta,\phi) &= r_0 + \sum_{\ell=2}^{\ell_{\max}} \sum_{m=-\ell}^{\ell} a_{\ell,m}\ R\ \mathrm{Y}_{\ell,m}(\theta,\phi), \\ \psi(\theta,\phi) &= \sum_{\ell=2}^{\ell_{\max}} \sum_{m=-\ell}^{\ell} b_{\ell,m}\ R^2\ \mathrm{Y}_{\ell,m}(\theta,\phi), \\ \chi(\theta,\phi) &= \sum_{\ell=2}^{\ell_{\max}} \sum_{m=-\ell}^{\ell} c_{\ell,m}\ R^2\ \mathrm{Y}_{\ell,m}(\theta,\phi). \end{aligned} \tag{S15}$$

Note that we excluded spherical harmonics with $\ell = 1$ that generate translations. The radial shrinking of shell r_0 is obtained from the fixed area constraint as

$$r_0 = -\frac{R}{16\pi} \sum_{\ell=1}^{\ell_{\max}} \sum_{m=-\ell}^{\ell} (\ell^2+\ell+2)|a_{\ell,m}|^2. \tag{S16}$$

The cutoff $\ell_{\max}$ is determined by requiring that the total number of degree of freedoms $3(\ell_{\max}+1)^2$ is equal to $3N-6$, where the 6 degrees of freedom are subtracted to prevent translations and translations. For a shell with $N = 72$ particles we consider $\ell_{\max} = 7$ and $\ell_{\max} = 8$.

The total deformation energy can be rewritten as [10]

$$\begin{aligned} U_\mathrm{b} + U_\mathrm{s} = \int dA \Bigg[& \frac{\kappa}{2}\left(\Delta f + \frac{2f}{R^2}\right)^2 + 2(\mu+\lambda)\frac{f^2}{R^2} + 2(\mu+\lambda)\left(\Delta\psi\right)\frac{f}{R} \\ & + \frac{(2\mu+\lambda)}{2}\left(\Delta\psi\right)^2 + \mu\frac{\psi\left(\Delta\psi\right)}{R^2} + \frac{\mu}{2}\left(\Delta\chi\right)^2 + \mu\frac{\chi\left(\Delta\chi\right)}{R^2}\Bigg]. \end{aligned}$$

$$\begin{aligned} U_\mathrm{b} + U_\mathrm{s} = \sum_{\ell=1}^{\ell_{\max}} \sum_{m=-\ell}^{\ell} \Bigg[& \left(\frac{\kappa}{2}(\ell+2)^2(\ell-1)^2 + 2(\mu+\lambda)R^2\right)|a_{\ell,m}|^2 - (\mu+\lambda)R^2\,\ell(\ell+1)\left(a_{\ell,m}b^*_{\ell,m} + a^*_{\ell,m}b_{\ell,m}\right) \\ & + \frac{R^2\ell(\ell+1)}{2}\left[(2\mu+\lambda)\ell(\ell+1) - 2\mu\right]|b_{\ell,m}|^2 + \frac{\mu R^2}{2}(\ell-1)\ell(\ell+1)(\ell+2)|c_{\ell,m}|^2\Bigg]. \end{aligned} \tag{S17}$$

The spectrum of fluctuations is thus

$$\begin{aligned} \left\langle |a_{\ell,m}|^2 \right\rangle &= \frac{k_B T}{\kappa(\ell+2)^2(\ell-1)^2 + YR^2\frac{(\ell+2)(\ell-1)}{\ell(\ell+1)-2\mu/(2\mu+\lambda)}}, \\ \left\langle |b_{\ell,m}|^2 \right\rangle &= \frac{k_B T}{(2\mu+\lambda)R^2\ell^2(\ell+1)^2 - 2\mu R^2\ell(\ell+1) - \frac{4(\mu+\lambda)^2R^4\ell^2(\ell+1)^2}{[\kappa(\ell+2)^2(\ell-1)^2+4(\mu+\lambda)R^2]}}, \\ \left\langle |c_{\ell,m}|^2 \right\rangle &= \frac{k_B T}{\mu R^2(\ell-1)\ell(\ell+1)(\ell+2)}. \end{aligned} \tag{S18}$$

The variance of radial fluctuations is

$$\left\langle \delta f^2 \right\rangle = \sum_{\ell=2}^{\ell_{\max}} \sum_{m=-\ell}^{\ell} R^2 \left\langle |a_{\ell,m}|^2 \right\rangle \equiv \frac{k_B T}{Y} G_N^f(\gamma),$$
$$G_N^f(\gamma) = \sum_{\ell=2}^{\ell_{\max}} \sum_{m=-\ell}^{\ell} \frac{\gamma}{(\ell+2)^2(\ell-1)^2 + \gamma \frac{(\ell+2)(\ell-1)}{\ell(\ell+1)-2/3}}, \tag{S19}$$

where we used $\mu = \lambda = 3Y/8$ that corresponds to the continuum limit of the OPS. Similarly, we calculate the variance of tangential fluctuations as

$$\left\langle \mathbf{u}^2 \right\rangle = \sum_{\ell=1}^{\ell_{\max}} \sum_{m=-\ell}^{\ell} R^2\, \ell(\ell+1) \left[\left\langle |b_{\ell,m}|^2 \right\rangle + \left\langle |c_{\ell,m}|^2 \right\rangle \right] \equiv \frac{k_B T}{Y} G_N^u(\gamma),$$
$$G_N^u(\gamma) = \sum_{\ell=2}^{\ell_{\max}} \sum_{m=-\ell}^{\ell} \left(\frac{8}{3\left[3\ell^2(\ell+1)^2 - 2\ell(\ell+1) - \frac{6\gamma\ell^2(\ell+1)^2}{(3\gamma+(\ell+2)^2(\ell-1)^2)} \right]} + \frac{8}{3(\ell-1)\ell(\ell+1)(\ell+2)} \right) \tag{S20}$$

In Fig. S1 we compare the scaling functions for radial displacements $G_N^f(\gamma)$ in Eq. (S19) and tangential displacements $G_N^u(\gamma)$ in Eq. (S20) for a shell with $N = 72$ particles ($\ell_{\max}$ = 7-8) to the ones obtained in the large shell limit ($G_\infty^f(\gamma)$ and $G_\infty^f(\gamma)$ in Eqs. (S12) and (S13) with $R/a = 2.2$). The radius $R = 2.2a$ was chosen, such that the area of the sphere is equal to the area of 140 equilateral triangles with side length a that are covering the surface of the shell with $N = 72$ particles, i.e. $4\pi R^2 = 140a^2\sqrt{3}/4$. Because the shell radius is quite small, we didn't use asymptotic expressions in Eqs. (S12b) and (S13b), but we numerically integrated expressions in Eqs. (S12a) and (S13a).

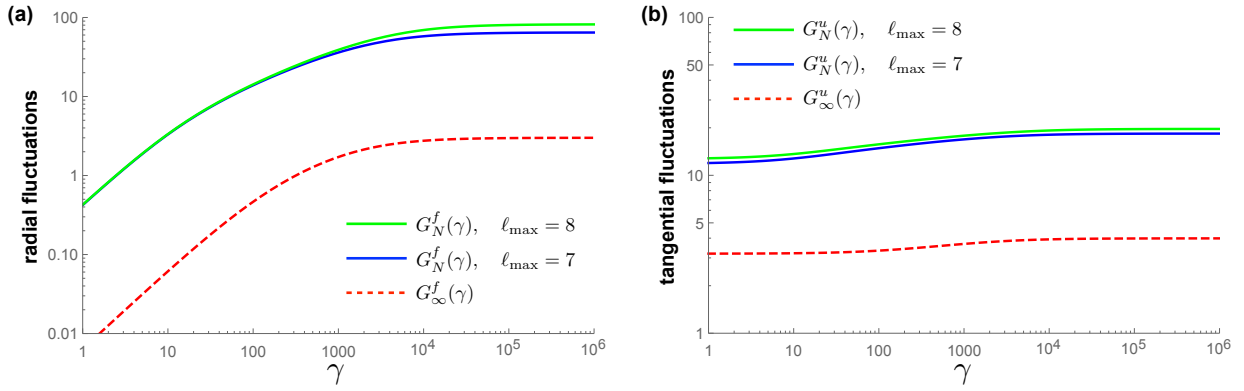

FIG. S1. Comparison of (a) radial fluctuations and (b) tangential fluctuations between the continuum theory for large thin shells (red dashed lines, $R/a = 2.2$) and finite size shells (blue, $\ell_{\max} = 7$, and green, $\ell_{\max} = 8$).

[1] K. Shoemake, "Animating rotation with quaternion curves," in *ACM SIGGRAPH computer graphics*, Vol. 19 (ACM, 1985) pp. 245–254.

[2] A. R. Singh, *Study of Zero and Finite Temperature Response of Discrete Deformable Surfaces*, Ph.D. thesis, UCLA (2018).

[3] W. Kabsch, "A solution for the best rotation to relate two sets of vectors," Acta Crystallogr. A **32**, 922–923 (1976).

[4] V. M. Bedanov, G. V. Gadiyak, and Y. E. Lozovik, "On a modified lindemann-like criterion for 2d melting," Phys. Lett. **109**, 289–291 (1985).

[5] The CGAL Project, *CGAL User and Reference Manual*, 4.14.1 ed. (CGAL Editorial Board, 2019).

[6] V. Borrelli, F. Cazals, and J. M. Morvan, "On the angular defect of triangulations and the pointwise approximation of curvatures," Comput. Aided Geom. Des. **20**, 319–341 (2003).

[7] C. Zhu, R. H. Byrd, P. Lu, and J. Nocedal, "Algorithm 778: L-bfgs-b: Fortran subroutines for large-scale bound-constrained optimization," ACM Trans. Math. Softw. **23**, 550–560 (1997).
[8] J. Paulose, G. A. Vliegenthart, G. Gompper, and D. R. Nelson, "Fluctuating shells under pressure," Proc. Natl. Acad. Sci. U.S.A. **109**, 19551–19556 (2012).
[9] A. Košmrlj and D. R. Nelson, "Statistical mechanics of thin spherical shells," Phys. Rev. X **7**, 011002 (2017).
[10] Z. Zhang, H. T. Davis, and D. M. Kroll, "Scaling behavior of self-avoiding tethered vesicles," Phys. Rev. E **48**, R651 (1993).